# Discrete Backbone Disorder in the Nuclear Magnetic Resonance Structure of Apo Intestinal Fatty Acid-Binding Protein: Implications for the Mechanism of Ligand Entry † , ‡

**ARTICLE** *in* BIOCHEMISTRY · MARCH 1997

Impact Factor: 3.02 · DOI: 10.1021/bi961890r · Source: PubMed



**2 AUTHORS**, INCLUDING:

David Cistola
University of North Texas HSC at Fort Worth
**68** PUBLICATIONS **2,951** CITATIONS

SEE PROFILE

# Discrete Backbone Disorder in the Nuclear Magnetic Resonance Structure of Apo Intestinal Fatty Acid-Binding Protein: Implications for the Mechanism of Ligand Entry[†,‡]

Michael E. Hodsdon and David P. Cistola*

*Department of Biochemistry and Molecular Biophysics, Washington University School of Medicine, St. Louis, Missouri 63110*

*Received July 30, 1996; Revised Manuscript Received December 4, 1996*[⊗]

ABSTRACT: The three-dimensional structure of the unliganded form of *Escherichia coli*-derived rat intestinal fatty acid-binding protein (I-FABP) has been determined using triple-resonance three-dimensional nuclear magnetic resonance (3D NMR) methods. Sequence-specific $^{1}$H, $^{13}$C, and $^{15}$N resonance assignments were established at pH 7.2 and 33 °C and used to determine the consensus $^{1}$H/$^{13}$C chemical shift-derived secondary structure. Subsequently, an eight-stage iterative procedure was used to assign the 3D $^{13}$C- and $^{15}$N-resolved NOESY spectra, yielding a total of 3335 interproton distance restraints or 26 restraints/residue. The tertiary structures were calculated using a distance geometry/simulated annealing algorithm that employs pairwise Gaussian metrization to achieve improved sampling and convergence. The final ensemble of NMR structures exhibited a backbone conformation generally consistent with the $\beta$-clam motif described for members of the lipid-binding protein family. However, unlike holo-I-FABP, the structure ensemble for apo-I-FABP exhibited variability in a discrete region of the backbone. This variability was evaluated by comparing the apo- and holoproteins with respect to their backbone $^{1}$H and $^{13}$C chemical shifts, amide $^{1}$H exchange rates, and $^{15}$N relaxation rates. Together, these results established that the structural variability represented backbone disorder in apo-I-FABP. The disorder was most pronounced in residues K29−L36 and N54−N57, encompassing the distal half of α-helix II, the linker between helix II and $\beta$-strand B, and the reverse turn between $\beta$-strands C and D. It was characterized by a destablization of long-range interactions between helix II and the C−D turn and a fraying of the C-terminal half of the helix. Unlike the solution-state NMR structure, the 1.2-Å X-ray crystal structure of apo-I-FABP did not exhibit this backbone disorder. In solution, the disordered region may function as a dynamic portal that regulates the entry and exit of fatty acid. We hypothesize that fatty acid binding shifts the order−disorder equilibrium toward the ordered state and closes the portal by stabilizing a series of cooperative interactions resembling a helix capping box. This proposed mechanism has implications for the acquisition, release, and targeting of fatty acids by I-FABP within the cell.

Intestinal fatty acid-binding protein (I-FABP)[1] is one of four homologous 14−16-kDa proteins expressed in the enterocytes of the small intestinal mucosa. It belongs to a family of intracellular lipid-binding proteins that bind fatty acids, retinoids, and sterols (Ockner *et al.*, 1972; Banaszak *et al.*, 1994; Veerkamp & Maatman, 1995). Given its binding properties and abundance in the apical cytoplasm of enterocytes, I-FABP is likely to function in the absorption, transcytoplasmic transport, and metabolic targeting of fatty acids derived from the diet. However, the specific metabolic roles of I-FABP are not well-defined, and the molecular mechanisms by which it facilitates lipid transfer through the cell remain unclear.

The three-dimensional structures of a number of intracellular lipid-binding proteins have been determined by X-ray crystallography and NMR spectroscopy (Sacchettini & Gordon, 1993; Banaszak *et al.*, 1994; Lassen *et al.*, 1995; Lücke *et al.*, 1996). We recently reported the $^{1}$H, $^{13}$C, and $^{15}$N NMR resonance assignments, chemical shift-derived secondary structure, and NOE-derived tertiary structure of I-FABP complexed with palmitate in solution (Hodsdon *et al.*, 1995, 1996). The tertiary structure was based on 3889 interproton distance restraints derived primarily from 3D $^{13}$C- and $^{15}$N-resolved NOESY experiments. The NOESY data were interpreted using an eight-stage iterative protocol based solely on the use of NMR data in order to avoid the introduction of bias from other structural models. In

[†]This work was supported by grants from the National Science Foundation (MCB-9205665 to D.P.C.) and the American Digestive Health Foundation and by institutional start-up funds. The Unity-500 spectrometer was supported in part by the Markey Center for Research in the Molecular Biology of Disease at Washington University. D.P.C. gratefully acknowledges a Johnson & Johnson/Merck Research Scholar Award from of the American Digestive Health Foundation.

[‡] The molecular coordinates for the two ensembles of NMR structures for apo- and holo-I-FABP have been deposited in the Brookhaven Protein Data Bank with ID numbers 1AEL and 1URE, respectively. Information about the DISTGEOM program and the TINKER molecular modeling package and instructions for downloading may be obtained at the the following web site: http://dasher.wustl.edu/ (128.252.162.151).

* To whom correspondence should be addressed: Campus Box 8231, Washington University School of Medicine, 660 South Euclid Ave., St. Louis, MO 63110-1093. Phone, 314-362-4382; Fax, 314-362-4153; E-mail, cistola@cosine.wustl.edu.

[⊗] Abstract published in *Advance ACS Abstracts,* January 15, 1997.

[1] Abbreviations: iLBPs, intracellular lipid-binding proteins; I-FABP, intestinal fatty acid-binding protein; HM-FABP, heart/muscle fatty acid-binding protein; A-LBP, adipocyte lipid-binding protein; I-LBP, ileal lipid-binding protein; NOE, nuclear Overhauser effect; NOESY, nuclear Overhauser and exchange spectroscopy; HSQC, heteronuclear single-quantum correlation spectroscopy; TINKER, a molecular modeling package for proteins developed by J. W. Ponder; DISTGEOM, a program within TINKER that implements the distance geometry algorithm employed in the present study; RMSD, root-mean-square deviation; CSI, chemical shift index.

S0006-2960(96)01890-9 CCC: $14.00 

addition, the structures were calculated using a novel distance geometry algorithm with improved sampling and convergence properties. Using this approach, the conformations of the protein backbone and the bound ligand in the NMR structure of I-FABP complexed with palmitate were found to be nearly identical to those observed in the corresponding X-ray crystal structure (Sacchettini *et al.*, 1989a; Hodsdon *et al.*, 1996).

The tertiary structure of I-FABP contains 10 $\beta$-strands arranged in an antiparallel, meandering topology. The first $\beta$-strand forms hydrogen bonds with the last, completing a flattened, clam-shaped $\beta$-barrel that houses an interior ligand-binding cavity. A helix−turn−helix domain is intercalated between the first and second $\beta$-strands and covers the otherwise open end of the $\beta$-barrel, separating the interior-bound ligand from the solvent. The mechanism by which fatty acid enters and exits the cavity has not been clearly established, but several hypotheses have been put forward. One hypothesis is that I-FABP contains a small opening or portal that allows the entry of ligand with minimal changes in the protein backbone conformation (Sacchettini *et al.*, 1989a,b). In this proposed mechanism, I-FABP is viewed as a molecular water pump that uses the displacement of ordered solvent molecules, rather than prominent conformational adjustments, to govern the binding of fatty acids (Sacchettini *et al*., 1992; Sacchettini & Gordon, 1993). This view was derived from a detailed comparison of the high-resolution X-ray crystal structures of I-FABP with and without bound fatty acid (Scapin *et al*., 1992; Sacchettini *et al*.,1992). The backbone conformations of the apo and holo forms of I-FABP are well ordered and nearly superimposable, with main-chain RMSD values of 0.4−0.6 Å. Similar results have been observed for the apo and holo crystal structures of cellular retinol binding proteins I and II (Cowan *et al*., 1993; Winter *et al*., 1993) and adipocyte lipid-binding protein (Xu *et al*., 1993).

A somewhat different hypothesis is that ligand binding is accompanied by a substantial change in protein backbone conformation (Jamison *et al.*, 1994). In this view, the apoprotein is thought to exist in one or more open, ligand-accessible states in solution, and ligand binding results in a conformational change leading to a more closed state. This hypothesis was initially based on the differing susceptibilities of several lipid-binding proteins to limited proteolysis in the presence and absence of ligand (Jamison *et al.*, 1994). Additional evidence for backbone conformational changes was provided by the unusual X-ray crystal structure of apo cellular retinoic acid-binding protein-I, which revealed a more open, ligand-accessible backbone conformation in the absence of ligand (Thompson *et al*., 1995). The open conformation of the apoprotein appears to be stabilized by the formation of intermolecular $\beta$-sheet interactions in the crystalline lattice, but it is unclear whether these interactions are relevant to the solution state. More recently, the properties of a helixless variant of I-FABP were characterized and compared with those of the wild-type protein (Kim *et al.*, 1996b; Cistola *et al.*, 1996). A rate-limiting process was observed in the association of oleate with wild-type I-FABP but not with the helixless variant, and this process was interpreted as a conformational change involving the helical region that allowed the ligand access to the internal cavity (Cistola *et al.*, 1996).

In the present study, we determined the three-dimensional structure of apo-I-FABP in solution using triple-resonance 3D NMR methods in order to gain further insight into the mechanism of fatty acid binding. The apo NMR structure was based on 3335 interproton distance restraints and was determined with protocols and sample conditions nearly identical with those used previously to characterize the holo-I-FABP complex with palmitate (Hodsdon *et al*., 1996). Unlike holo-I-FABP, the NMR solution structure of apo-I-FABP is different from the corresponding X-ray crystal structure and exhibits a discrete region of backbone disorder in solution. This disorder is most pronounced in residues 29−36 and 54−57 and is characterized by a decoupling of interactions between α-helix II and the C−D turn and a fraying of the helix at its C-terminal end. The apparent disorder observed in the chemical shift- and NOE-derived NMR structures was independently verified by comparing the amide $^1$H saturation transfer rates and $^{15}$N relaxation rates for the apo- and holoproteins (Hodsdon & Cistola, 1997). We propose that apo-I-FABP in solution exists as a manifold of locally disordered and ordered states in equilibrium and that the binding of ligand stabilizes a series of cooperative interactions that shift the equilibrium toward the ordered state. These long-range cooperative interactions in I-FABP resemble the short-range helix capping interactions thought to stabilize the C-termini of α-helices in many proteins (Aurora *et al.*, 1994). The NMR results lead to a revised hypothesis regarding the mechanism of ligand acquisition and release by I-FABP and its possible role in regulating fatty acid transfer and targeting within the cell.

## MATERIALS AND METHODS

*Sample Preparation.* To facilitate the comparison of apo- and holo-I-FABP, the apo NMR samples for the current study were prepared using the same batch of protein, except for the lack of bound fatty acid, that was used for the determination of the solution structure of I-FABP complexed with bound palmitate (Hodsdon *et al.*, 1996). The biosynthesis, purification, and delipidation of [88% U-$^{13}$C, 99% U-$^{15}$N]-I-FABP have been detailed elsewhere (Hodsdon *et al.*, 1995). The completeness of delipidation was verified by 2D $^1$H/$^{15}$N HSQC, as described in Hodsdon and Cistola (1997). The final protein concentration was 2 mM with a buffer containing 20 mM potassium phosphate, 50 mM potassium chloride, and 0.05% sodium azide, pH 7.2, and the samples contained either 20% $D_2O$ ("$H_2O$ sample") or 99.996% $D_2O$ ("$D_2O$ sample").

*NMR Spectroscopy*. The triple-resonance 3D NMR spectra used to establish sequence-specific $^1$H, $^{13}$C, and $^{15}$N resonance assignments and determine the solution structure of apo-I-FABP were acquired, processed, and referenced as previously described (Hodsdon *et al.*, 1995, 1996) with the following exceptions. First, GARP-1 (Shaka *et al.*, 1985) was utilized to acheive broad-band decoupling of the 15-kHz $^{13}$C spectral window instead of MPF10 (Fujiwara *et al.*, 1993). This decoupling was applied during the $t_1$ and $t_3$ time domains of the 3D $^{13}$C−NOESY−HSQC experiment. As reported by Fujiwara *et al.* (1993), MPF10 decoupling requires relatively higher RF power to suppress cycling side bands. Such side bands complicate the analysis of a $^{13}$C-resolved NOESY spectrum because of the intense diagonal. Second, the NMR spectra were collected at 33 °C instead of 37 °C because apo-I-FABP slowly precipitated at the

higher temperature. The 4 °C decrease in temperature minimized the loss of protein due to aggregration with only very minor effects on the chemical shifts. To rule out the unlikely possibility that the 4 °C temperature difference might have accounted for the observed differences in apo- and holo-I-FABP, the subsequent relaxation and exchange experiments were performed under identical conditions suitable for both apo- and holo-I-FABP (25 °C, 2 mM protein; Hodsdon & Cistola, 1997). Neither protein exhibited any sign of aggregation under those conditions. Both apo- and holo-I-FABP yielded spectra with backbone amide $^{1}H$ and $^{15}N$ line widths consistent with 15-kDa monomers under all sample conditions employed.

*Resonance Assignments*. The assignment strategy for apo-I-FABP employed six of the seven 3D triple-resonance experiments previously used to assign holo-I-FABP. The seventh experiment, CC-TOCSY, was unnecessary in the present case since the holo assignments provided an approximate starting point for choosing appropriate $^{13}C$ planes in the HCCH-TOCSY experiment for apo-I-FABP. The assigment strategy and protocols were otherwise identical to those previously employed (Hodsdon *et al*., 1995, 1996).

*Restraint Derivation and Structure Calculations*. Interproton distance restraints were derived primarily from two 3D $^{13}C$- and $^{15}N$-resolved NOESY NMR spectra. Because of the significant ambiguity encountered in interpreting or assigning 3D NOESY spectra of this 15-kDa protein, an iterative procedure was utilized for the succesive interpretation of the cross peaks and the generation of structure families (Hodsdon *et al.*, 1996). The first step of this procedure relied critically on the combined use of the $^{1}H/^{13}C$ chemical shift-derived secondary structure and the symmetry-checked, "pseudo-4D" restraints from the 3D $^{13}C$-resolved NOESY experiment. Together, this information established the topology of I-FABP and provided an initial structural model for interpreting the NOESY data. The first set of 907 interproton distance restraints served as input for the calculation of an ensemble of imprecise but accurate tertiary structures that established the global fold. This initial ensemble was then used to reinterpret the NOESY data leading to further cycles of structure calculations and assignments. Distance restraints to some aromatic ring protons were identified from a 2D NOESY spectrum using the NMR structure ensembles as a guide and were incorporated into the middle stages of the iterative procedure. For reasons discussed elsewhere, the NOE data were interpreted in a conservative manner and each restraint was given an upper bound of 5 Å plus any prochiral corrections (Hodsdon *et al*., 1996).

All structure calculations were performed on a Silicon Graphics INDY/R4400 workstation using a distance geometry/simulated annealing algorithm implemented in the TINKER protein modeling package. This software package contains the program DISTGEOM, which has the option of implementing distance geometry with pairwise Gaussian metrization. The unique features of this algorithm and the protocols used for embedding and refining structures have been detailed elsewhere (Hodsdon *et al.*, 1996).

## RESULTS

*Resonance Assignments and Chemical Shift-Derived Secondary Structure*. Complete backbone and side-chain aliphatic $^{1}H/^{13}C$ assignments were established for 123 of the 131 residues of apo-I-FABP. Because of the rapid exchange of some amide hydrogens with solvent at pH 7.2 and 33 °C, backbone $^{1}H/^{15}N$ resonances were not observed for 23 residues. In a subsequent study, we were able to observe 11 of these 23 by using gradient- and sensitivity-enhanced pulse sequences and by decreasing the temperature from 33 to 25 °C (Hodsdon & Cistola, 1997). These positions of "missing" amide resonances in spectra of apo-I-FABP, but not holo-I-FABP, provided supportive evidence for the localized backbone disorder (see below). The current $^{1}H$, $^{13}C$, and $^{15}N$ resonance assignment tables for rat I-FABP in the presence and absence of bound palmitate are available as supporting information.

The solution secondary structure of apo-I-FABP was determined directly from the chemical shift assignments using the consensus $^{1}H/^{13}C$ chemical shift index described by Wishart and Sykes (1994). A key advantage of this approach is that the secondary structure can be accurately determined without NOEs, which are initially ambiguous and difficult to interpret for larger proteins. Definition of the secondary structure dramatically reduces the number of possible folds that the protein can adopt and facilitates the initial assignment of otherwise ambiguous NOESY cross-peaks. Plotted in Figure 1 are CSI values for the $H_\alpha$, $C_\alpha$, CO, and $C_\beta$ resonances of apo-I-FABP. The consensus CSI, formulated from these four individual sets, are shown below. The consensus CSI values of $+1$, $-1$, and 0 are indicative of $\beta$-strands, α-helices, and unstructured regions or turns, respectively (Wishart & Sykes, 1994). For comparative purposes, the consensus CSI and a graphical representation of the secondary structure of holo-I-FABP are displayed at the bottom of the figure. The largest differences between apo- and holo-I-FABP were noted in the distal half of α-helix II. In the apoprotein, this segment appeared to be less structured, on average, as compared with the holoprotein. Comparison of the chemical shift values for each of the four nucleus types indicated that the greatest apo/holo differences resided in the $C_\alpha$ and CO values [cf. Figure 1 with Figure 8 of Hodsdon *et al*. (1995)]. In other regions of the protein, the consensus CSI maps were nearly the same for apo- and holo-I-FABP. Some minor differences were noted at the boundaries of secondary structure elements.

At the top of Figure 1, the locations of rapidly exchanging amide hydrogens are compared along the protein sequence for apo- and holo-I-FABP, as defined by their absence in NMR spectra collected at pH 7.2 and 33 or 37 °C and using presaturation of the water resonance for solvent suppression. Unlike holo-I-FABP, amide proton resonances were selectively absent in spectra of apo-I-FABP at positions corresponding to the beginning of α-helix I, the C-terminal portion of α-helix II and the proceeding linker, and the turns between $\beta$-strands C−D and E−F. Similar differences have been observed for the amide proton resonances of apo and holo cellular retinoic acid-binding protein I, although the apo and holo forms were characterized at different pH values: pH 3.8 and 7.5, respectively (Rizo *et al*., 1994).

*NOE-Derived Ensemble of Tertiary Structures.* Table 1 lists the statistics for the final set of conformational restraints used for the structure calculations. The distribution of the distance restraints along the sequence of the protein is plotted in Figure 2A. In order to facilitate comparison of the

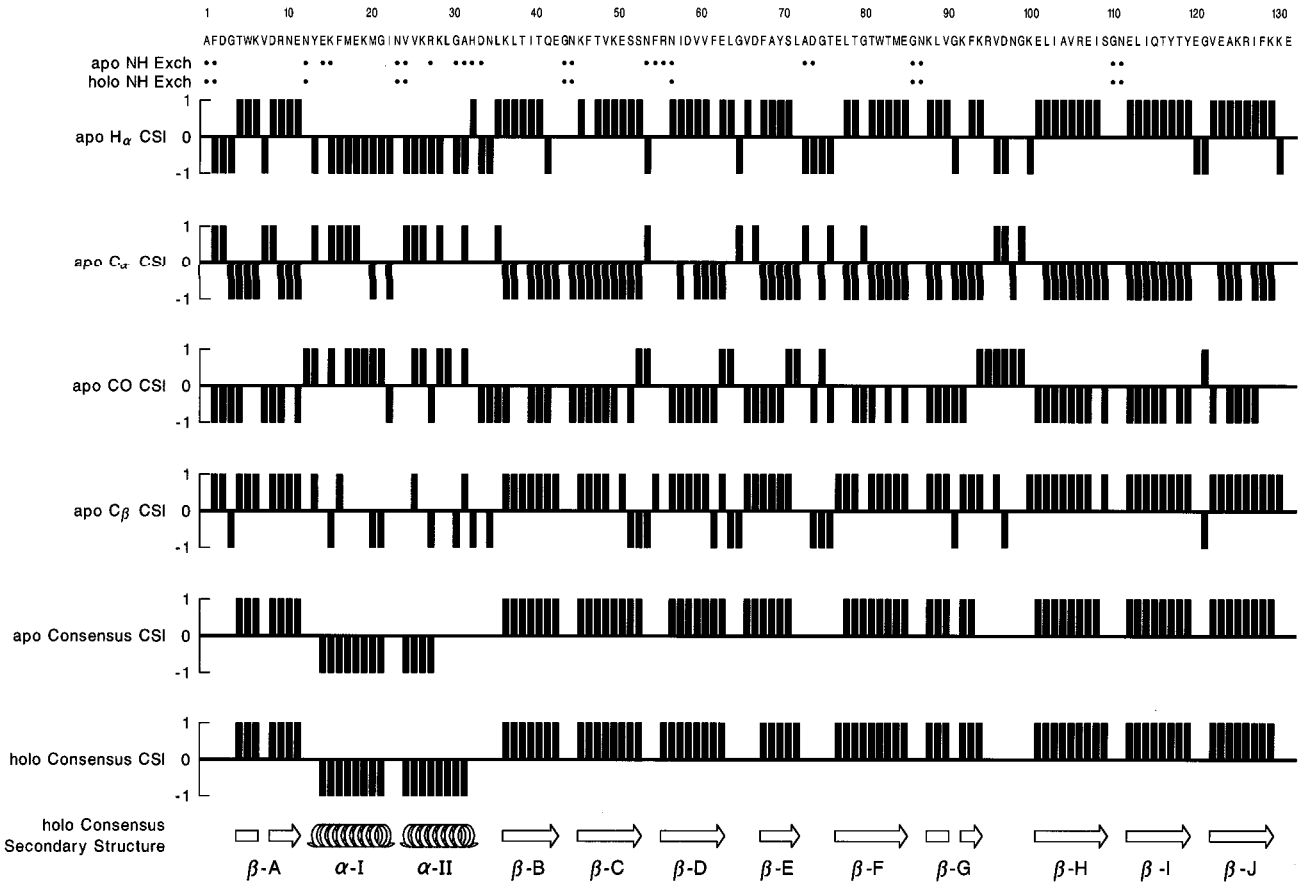


FIGURE 1: Chemical shift indices (CSI) for the $H_\alpha$, $C_\alpha$, $C_\beta$, and CO resonances and the resulting consensus CSI for apo-I-FABP, are plotted along the protein sequence. For comparison, the consensus CSI and solution secondary structure of holo-I-FABP (Hodsdon *et al.*, 1995) are also included. The location of rapidly exchanging amide hydrogens for apo- and holo-I-FABP are designated by filled circles (see Results). In most cases, the absence of a bar represents a CSI value of 0, consistent with unstructured protein. Exceptions include residues 15, 24, 44, 56, 86, 87, 110, and 111, for which backbone assignments were not available. The raw chemical shift data are provided as supporting information.

Table 1: Final Restraint Statistics for Apo-I-FABP

| | |
|---|---|
| **Distance Restraints** | |
| total | 3335 (25.5/residue) |
| intraresidue | 686 |
| sequential ($i$, $i \pm 1$) | 682 |
| medium-range ($i$, $i \pm 2$, $i \pm 3$, $i \pm 4$) | 433 |
| long-range | 1534 |
| **Torsional Restraints**[a] | |
| helical Φ/Ψ restraints | 12 |
| **Restraint Violations**[b] | |
| upper bounds | |
| average violation (Å) | $0.02 \pm 0.02$ |
| largest violation (Å) | 0.09 |
| no. of violations | 63 of 66 700[c] (0.09%) |
| lower bounds | |
| average violation (Å) | $0.08 \pm 0.06$ |
| largest violation (Å) | −0.30 |
| no. of violations | 123 of 66 700[c] (0.2%) |

[a] Derived from consensus chemical shift indices in Figure 1. The use of these restraints prevented the α-helices from getting trapped in local minima during simulated annealing (Hodsdon *et al.*, 1996). Dihedral restraints were not enforced for the β-strand segments and were not necessary for obtaining converged structures. [b] Analyzed using AQUA version 0.40 and PROCHECK-NMR version 3.4.2 (Rullman, 1996; Laskowski *et al.*, 1993). [c] The product of the number of restraints and the number of structures in the final ensemble.

structural results for apo- and holo-I-FABP, the difference in the number of NOE-derived distance restraints for each residue is shown in Figure 2B. A negative value represents the observation of fewer restraints for apo-I-FABP.

The final ensemble of 20 NMR structures for apo-I-FABP is displayed in Figure 3 as a stereo plot of backbone $C_\alpha$ traces. The penalty function values of the ensemble were $3.7 \pm 0.5$; values less than 10 indicate good agreement with the experimental restraints (Hodsdon *et al.*, 1996). The final restraint violation statistics are also listed in Table 1. Because of the high convergence rate, all 20 structures calculated using the final set of restraints were accepted and none were discarded. The RMSD values for this final ensemble were calculated in several different ways and are listed in Table 2.

A quantitative description of conformational variability within the family of NMR structures, a comparison of the two ligation states of I-FABP, and a comparison to their respective X-ray crystal structures was provided by an analysis of the average deviations of atomic coordinates. Figure 4A displays the residue distribution of average pairwise $C_\alpha$ deviations for the family of superposed NMR structures shown in Figure 3. The plot of average deviations, calculated as the average of the distances between atomic coordinates for every pair of individual structures, illustrates the distribution of structural heterogeneity along the protein backbone. In a similar manner, the entire family of NMR structures can be compared to the X-ray crystal structure of apo-I-FABP (Figure 4B) and to the family of holo-I-FABP NMR structures (Figure 4C).

The structural and stereochemical quality of the final ensemble of apo-I-FABP NMR structures was analyzed using

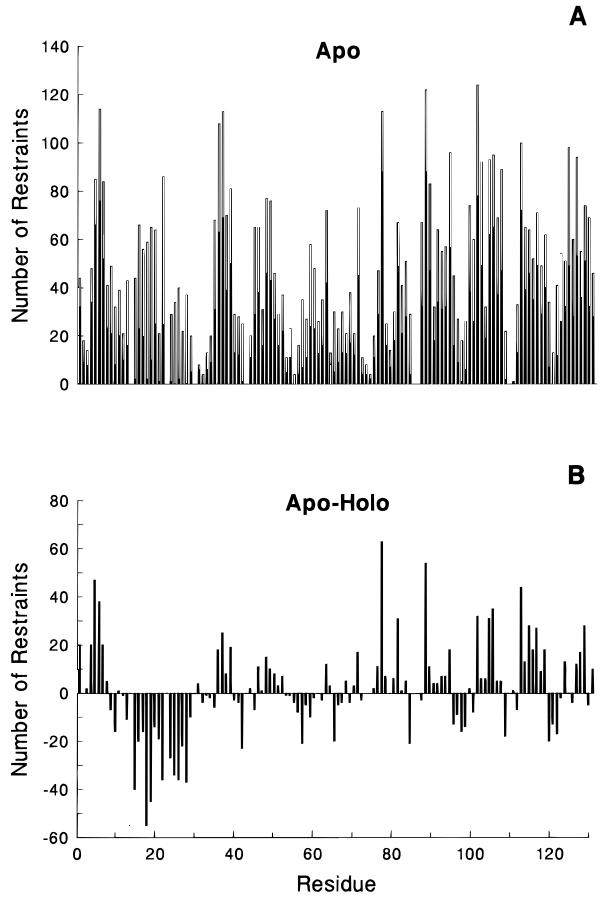


FIGURE 2: (A) Distribution of total (open bars) and long-range (closed bars) distance restraints used for the calculation of the final ensemble of apo-I-FABP NMR structures. Long-range distance restraints are defined as $|i - j| > 4$, where $i$ and $j$ are residue numbers in the sequence. In this plot, each interresidue restraint is allotted twice, once for each of the dipolar-coupled partners. (B) Difference in total restraints obtained for apo- and holoprotein, such that fewer restraints observed for apo results in a negative value.

PROCHECK-NMR (Laskowski *et al.*, 1993) as summarized in Table 2. Statistics are provided for the subdivision of backbone $\phi/\psi$ dihedral angles into variously favored regions of the Ramachandran plot and for a variety of other main- and side-chain parameters. The specific meaning and significance of these parameters are discussed in Morris *et al*. (1992). On average, 91% of the residues were found in allowed regions of the Ramachandran plot and 36% of the residues were in the most favored regions. Note that the family of NMR structures at this stage were deliberately refined with a limited penalty function lacking a general torsional energy term (Hodsdon *et al*., 1996). The inclusion of such a term would be expected to localize backbone torsions to generally more favorable values. As well, a significant portion of the protein backbone was disordered in the family of apo-I-FABP NMR structures (see Discussion) and might not be expected to be restrained to the most favored regions of $\phi/\psi$ space. The values of the main-chain statistics are generally comparable to those typical of 2.5-Å crystal structures, although such comparisons may be misleading in the context of dynamic disorder in the solution state. The side-chain values indicate that they are currently not as well-defined as the backbone. This result is not unexpected since stereospecific assignments have not yet been incorporated, and the upper bounds for a number of distance restraints involving prochiral side-chain atoms are quite large (Hodsdon *et al*., 1996).

## DISCUSSION

Rat I-FABP is currently the only member of the iLBP family whose NMR structures have been determined in both the liganded and unliganded states. Thus, the comparison of these structures provides a unique opportunity to assess the effect of the bound ligand on the structural and dynamical properties of the protein in solution. High-resolution X-ray crystal structures of rat apo- and holo-I-FABP have also been determined, and thus, detailed comparisons can also be made between the properties of the protein in the crystalline and solution states.

In the current study, the solution structure of apo-I-FABP was determined using 3335 interproton distance restraints representing an average of 26 total and 12 long-range restraints/residue. The global fold is generally consistent with the $\beta$-clam motif observed for proteins in the intracellular lipid-binding protein family. However, there are several significant differences, the most striking of which is a localized region of increased variability within the ensemble. The average pairwise $C_\alpha$ RMSD for the 20 superposed NMR structures is 1.17 Å, as calculated for the entire protein sequence (Table 2). The distribution of average pairwise $C_\alpha$ deviations in Figure 4A indicates values between 0.5 and 1.0 Å for many residues, consistent with well-defined structure (Havel, 1991; Hodsdon *et al*., 1996). However, some residues exhibit larger deviations, with the largest values clustered in two segments of the protein sequence. The first segment involves residues N24−L36, corresponding to the second α-helix and the preceding linker, with the maximum deviations in residues 29−34. The second segment involves residues N54−N57, corresponding to the turn between $\beta$-strands C and D, specifically. These two segments of the protein sequence are adjacent in the tertiary structure and represent a single region of apparent disorder in solution.

Supporting evidence for a discrete region of backbone disorder in apo-I-FABP was provided by chemical shift values and the location of rapidly exchanging amide hydrogens (Figure 1). The $^1H/^{13}C$ consensus chemical shift index indicated that, on average, the second α-helix extended only one turn from residues V25 through R28 followed by a less structured region from K29 to L36. In contrast, helix II in the holoprotein extended four more residues through A32. In addition, the backbone amide hydrogen exchange rates were more rapid for apo-I-FABP at positions 28, 31−34, 54−56, and 73∠74, as inferred by comparing the patterns of amide proton resonances selectively absent in corresponding spectra of apo-I-FABP but not holo-I-FABP.

The smaller number of $^{13}C$-NOESY-derived restraints in this region of apo-I-FABP provided evidence that the local structural variability was not simply the result of the selective saturation of amide resonances in the $^{15}N$-NOESY spectrum. Specifically, residues 24−36 and 54−57 exhibited a total of 531 $^{13}C$-NOESY-derived restraints for holo-I-FABP but only 329 for apo-I-FABP. For comparison, the $\beta H-\beta I$ region encompassing residues 101−119 exhibited a comparable number of $^{13}C$-NOESY-derived restraints for the holo- and apoproteins: 954 and 998, respectively.

In a related study, we characterized and compared the backbone mobility of apo- and holo-I-FABP by measuring

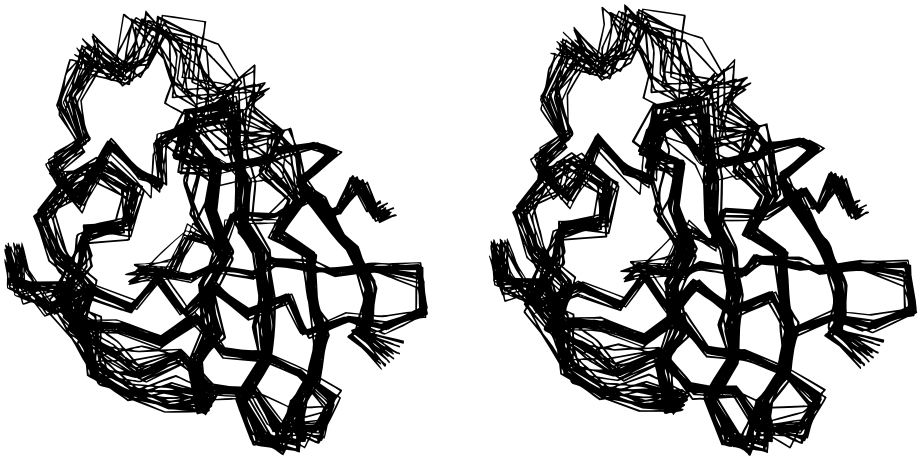

FIGURE 3: Stereo diagram of 20 superposed backbone $C_\alpha$ traces representing the final ensemble of NMR structures for apo-I-FABP. These structures were calculated using the distance geometry/simulated annealing protocol described elsewhere (Hodsdon *et al*., 1996). The average pairwise $C_\alpha$ RMSD for this family is 1.2 Å. This figure, as well as Figures 5 and 6, were generated using MOLSCRIPT (Kraulis, 1991).

Table 2: Structural and Stereochemical Statistics for Apo-I-FABP[a]

| ensemble RMSD values | all residues | ordered residues[b] |
|---|---|---|
| average pairwise $C_\alpha$ RMSD (Å) | 1.17 | 0.85 |
| average main-chain RMSD from mean coordinates (Å) | 0.92 | 0.71 |

| statistic | ensemble average |
|---|---|
| Ramachandran Plot Statistics | |
| residues in allowed regions | 106 (91%)[c] |
| most favored regions | 42 (36%) |
| additionally allowed regions | 45 (39%) |
| generously allowed regions | 19 (16%) |
| residues in disallowed regions | 11 (9%) |
| Main-Chain Statistics | |
| standard deviation of $\omega$ (deg) | 2.3 |
| no. of bad contacts/100 residues | 13.9 |
| standard deviation of "Zeta-angle" (deg) | 4.5 |
| standard deviation of H-bond energy (kcal/mol) | 0.8 |
| deviations from ideal bond lengths[d] (Å) | $0.006 \pm 0.003$ |
| deviations from ideal bond angles[d] (deg) | $1.11 \pm 0.79$ |
| Side-Chain Statistics[e] | |
| $\chi$1 gauche minus | 29.5 |
| $\chi$1 trans | 30.2 |
| $\chi$1 gauche plus | 29.4 |
| $\chi$1 "pooled" | 30.6 |
| $\chi$2 trans | 27.9 |

[a] These analyses, except for the calculation of average pairwise $C_\alpha$ RMSD values, were performed using PROCHECK version 3.4.2 (Laskowski et al., 1993). The meaning and significance of these statistics are discussed in Morris *et al*. (1992). [b] Defined as 1−23, 37−52, 58−70, and 77−131. This analyses excludes the residues determined to be disordered in apo-I-FABP based on a consensus of the structural and dynamical results [Figure 8 of Hodsdon and Cistola (1997)]. [c] Based on a total of 117 non-Gly/non-Pro residues. [d] Mean values ±SD of values for 8 categories of bond lengths and 13 categories of bond angles. [e] Standard deviations in degrees.

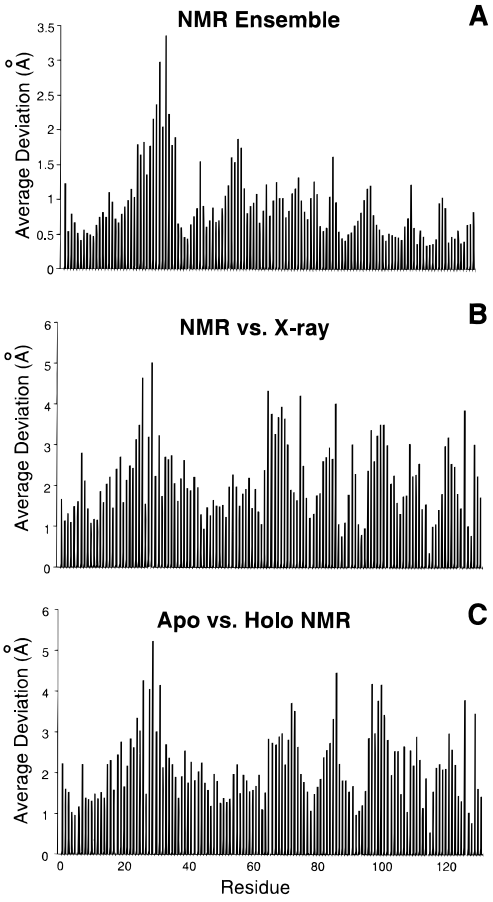


FIGURE 4: Distributions of the average $C_\alpha$ deviations along the sequence of the protein for the apo-I-FABP NMR ensemble (A), its comparison to the X-ray structure (B), and for the comparison of apo- and holoproteins (C). The *y*-axis represents the pairwise average deviation of the $C_\alpha$ coordinates calculated for every possible pair of superposed structures. In panel A, the comparison is made for every pair of structures in the final NMR ensemble. In panels B and C, the comparison is made for the average of the deviations between each NMR structure and the crystal structure or each member of the holo-I-FABP NMR ensemble, respectively.

amide $^{15}$N relaxation and $^{1}$H saturation transfer rates at 25 °C (Hodsdon & Cistola, 1997). Residues in the vicinity of helix II and the C−D and E−F turns were characterized by low order parameters, sizeable exchange terms, and higher rates of saturation transfer, particularly in the apo state. The remainder of the protein was characterized by high order parameters, small or vanishing exchange terms, and low rates of saturation transfer in both apo- and holoproteins. Thus, dynamical results reinforced the observations from the chemical shift- and NOE-derived structures and indicated that the local variability in the ensemble of apo NMR structures represents increased backbone disorder and mobility in a specific region of the protein.

NMR structures have been determined for two other members of the iLBP family: the holo form of bovine heart/muscle fatty acid-binding protein (Lassen *et al*., 1995) and the apo form of porcine ileal lipid-binding protein (Lücke

*et al.*, 1996). These proteins are 30% and 21% identical with rat I-FABP at the sequence level, respectively, and exhibit essentially the same global fold. Like I-FABP, HM-FABP also binds a single molecule of fatty acid, although in a different conformation and location. In contrast, I-LBP binds fatty acids or bile salts but prefers the latter. The NMR structure ensembles for holo HM-FABP and apo I-LBP both exhibited variability somewhat similar to that shown here for apo-I-FABP. Thus, it is possible that backbone disorder in this region of the protein is a common feature of members of this protein family. However, it is not clear whether the variability in the structure ensembles for holo-HM-FABP and apo I-LBP represents true disorder, since their backbone relaxation and dynamical properties have not yet been characterized. In addition, the NMR structures for each protein have not yet been determined in both the apo and holo states. More studies are necessary to further evaluate the similarities and differences between these three related proteins.

*Comparison of the NMR and X-ray Crystal Structures of Apo-I-FABP*. In contrast to the NMR results, backbone disorder was not observed in the 2.0- and 1.2-Å X-ray crystal structures of apo-I-FABP (Sacchettini *et al.*, 1989b; Scapin *et al.*, 1992).[2] The main-chain temperature factors for residues 24−36 and 54−57 were low and not significantly different from those for the rest of the protein backbone (see 1ifc; Brookhaven Protein Data Bank). Also, unlike the NMR structures, the backbone conformations of the apo and holo crystal structures were nearly superimposable, with main-chain RMSD values of 0.4 Å. There are no obvious or direct protein−protein contacts in the crystalline lattice that might explain the ordering of this portion of the molecule and the apparent differences between the NMR and X-ray results. The sample conditions used to favor crystallization may have shifted the order−disorder equilibrium toward the ordered state or the crystallization process may have selected for a state with an ordered backbone.

The backbone conformation of the NMR and X-ray structures of apo-I-FABP are compared as traces through the $C_\alpha$ coordinates in Figure 5 (left panel) and as ribbon diagrams in Figure 6. These structures have both an overall similarity and specific, local differences. The average pairwise $C_\alpha$ RMSD between the ensemble of NMR structures and the X-ray crystal structure is 2.3 Å. The variability in the region around the second helix contributes significantly to this value, as seen in Figure 4B. However, the X-ray structure appears to approximate an average conformation within the disorder, and therefore, there are only a few large average deviations between the two models in this region. A large difference in the average conformation is apparent in $\beta$-strand E and the proximal portion of strand F. This segment corresponds to the lower left portion of the molecule as shown in the left panel of Figure 5. Distance restraints

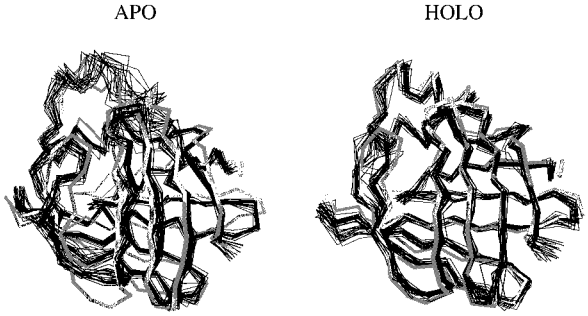


FIGURE 5: Comparison of the NMR ensembles (thin black lines) of apo- and holo-I-FABP and their respective X-ray structures (thick gray lines). The currently reported family of apo-I-FABP NMR structures and the 1.2-Å X-ray structure (Scapin *et al.*, 1992) are shown on the left. On the right is shown the family of holo-I-FABP NMR structures (Hodsdon *et al.*, 1996) and the 2.0-Å X-ray structure (Sacchettini *et al.*, 1989a).

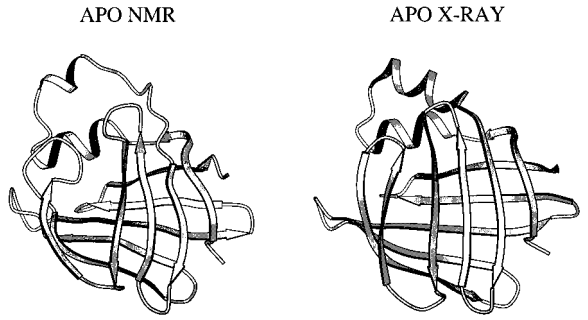


FIGURE 6: Ribbon diagrams representing a single selected NMR structure from the ensemble of apo-I-FABP NMR structures in Figure 3 and the X-ray crystal structure of Scapin *et al.* (1992). In the NMR structure, the positions of the secondary structure elements were defined by the consensus $^1H/^{13}C$ CSI for apo-I-FABP, as in Figure 1.

inconsistent with the conformation of the X-ray crystal structure were observed for A69−S71, resulting in a widening of the gap between $\beta$-strands D and E. Near the E−F turn, restraints between L72 and hydrophobic residues within the cavity (L78, L102, F17, and M18) draw the distal portion of $\beta$-strand E and a portion of the E−F turn into the unoccupied cavity. Overall, these conformational differences result in a shift in the position of most of $\beta$-strand E and the initial portion of $\beta$-strand F (Figure 6). The changes in this region of the NOE-based apo structure compared with the holo structure are consistent with the CSI observation of a larger segment of nonregular secondary structure from L72−E77 and the selective absence of amide proton resonances for A73 and D74 (Figure 1).

The gap between $\beta$-strands D and E is a common feature of the $\beta$-clam motif and has been observed in all other known structures of iLBPs. Unlike strands in a typical $\beta$-sheet, strands D and E do not form direct hydrogen bonds between their corresponding main-chain atoms. Instead, interstrand interactions between side-chain atoms, sometimes involving bridging water molecules, serve to fill the gap. Young *et al.* (1994) have proposed, mainly on the basis of an analysis of the crystallographic data for HM-FABP, that a secondary portal for the displacement of solvent from the interior cavity during ligand binding is located in this region. In the NMR structure for apo-I-FABP, the markedly widened gap between strands D and E does appear to create a small opening into the interior cavity. The apparent opening is centered between the aromatic rings of F68 and Y70. However, minor

[2] The term "discrete disorder" was used to describe the alternative positions of some atoms in the 1.2-Å X-ray crystal structure model of apo-I-FABP [footnote 5 of Scapin *et al.* (1992)]. However, this type of structural heterogeneity is fundamentally different, in both character and location, from the backbone disorder described here. Twenty-two residues were listed as exhibiting dual conformations in the crystal structure (16, 17, 29, 35, 45−47, 55, 70, 81, 85−87, 93, 107, 113, 114, 117, 118, 123, 125, and 127), but only three of those residues are located in the discrete region of backbone disorder observed in the present study (24−36 and 54−57).

rotations of the $\chi 1$ dihedral angles of these residues are sufficient to close the opening. Many interstrand NOE correlations were observed for the side-chain atoms of these residues; specifically, there are four restraints between F68 and F62 and six restraints between Y70 and residues I58 and V60. Because of the lack of stereospecific assignments of the side-chain aliphatic and aromatic hydrogens, the large upper bounds of these restraints limit the precision of localizing the side-chain positions in our current NMR structures of I-FABP. Hence, it is not yet known whether the apparent opening seen in many of the apo NMR structures is significant or not. Further evaluation will require a refinement of the side-chain positions made possible by stereospecific assignments.

The NMR and X-ray crystal structures of apo-I-FABP appear quite similar in the C-terminal region encompassing $\beta$-strands G−J. The superposition of the NMR ensemble with the crystal structure shown in Figure 5 was based on a least-squares fit to the RMSD which gives a relatively higher weight to regions of dissimilarity. This results in a poorer superposition of the sections of similar structure than is possible if the exceptional differences are not considered. A repeat of the superposition with the exclusion of the disordered or dissimilar residues (29−36, 54−57, and 64−79) showed an improved RMSD of 2.1 Å. Most of the remaining differences involve the turns between $\beta$-strands G and H and between I and J. In the X-ray structure, these residues are involved in crystal packing contacts which may affect their position.

*Comparison of the Apo and Holo NMR Structures of I-FABP*. Figure 5 compares the two ensembles of NMR structures along with their corresponding X-ray crystal structures. In contrast to apo-I-FABP, holo-I-FABP appears globally well-ordered and nearly identical with its X-ray structure (Hodsdon *et al*., 1996). The most striking and unique feature of the apo NMR structure, as detailed above, is the disorder observed in the distal half of α-helix II, the α-II/$\beta$-B linker, and the C-D turn. The deviations between the $C_\alpha$ coordinates of the two families of NMR structures, visible in Figure 5 and plotted in Figure 4C, mirror the differences between the family of apo-I-FABP NMR structures and the apo crystal structure as discussed above. This result is expected considering the good agreement between the NMR and X-ray results for holo-I-FABP and the nearly identical backbone conformations of the apo and holo X-ray structures.

In the absence of ligand, the conformation of apo-I-FABP in solution can be subdivided into two general regions based upon the degree of structural heterogeneity observed in the family of NMR structures. This subdivision mirrors the differential interactions of bound palmitate with protein side chains (Sacchettini *et al.*, 1989a). The carboxylate terminus and the concave face of the fatty acid chain primarily interact with ordered water molecules and polar side-chain atoms in the cavity. These interactions are generally located toward the middle and lower right of the protein structure as displayed in Figure 3. This region consists of most of the amino acids in $\beta$-strands A−D and G−J, with the exception of the C−D, G−H, and I−J turns, and is well-ordered in both the apo- and holo-I-FABP NMR structures. It includes residues in the vicinity of W82 and the hydrophobic core of I-FABP, postulated to form as an early event in the folding pathway (Ropson & Frieden, 1992). The second region includes residues toward the left side of the molecule as displayed in Figure 3. This region appears more disordered in the absence of ligand, as seen in the apo/holo comparison in Figure 5. In this locale, the bound palmitate is primarily involved in hydrophobic interactions with protein side chains.

The polar face of the internal ligand-binding cavity appears to be a conserved feature within the family of lipid-binding proteins. A similar network of ordered solvent and polar side-chains atoms interacting with a portion of bound fatty acid has been observed for I-FABP, HM-FABP, and A-LBP (Sacchettini *et al.*, 1989a; Scapin *et al.*, 1992; Xu *et al.*, 1993; LaLonde *et al*., 1994; Young *et al.*, 1994). In all cases, the ordered solvent molecules and their coordinating side-chain atoms are found in nearly identical positions both in the absence of ligand and with a variety of bound lipids. Hence, they are thought to represent an integral component of the structural framework of the interior cavity. It has been postulated that this internal solvent structure acts to regulate the conformation of the ligand-binding cavity and, therefore, the conformational space available to the bound fatty acid. This proposed regulation would contribute to the mechanism of lipid-binding specificity within the family. The conserved, stable solvent structure may also act to maintain the integrity of the solvent-filled internal cavity in the absence of ligand. The well-ordered conformation seen for the polar face of the cavity in both the apo and holo NMR structures provides additional support for these hypotheses.

*Implications for the Mechanism of Ligand Binding.* The present NMR results, interpreted in the context of other findings for I-FABP and related proteins, led us to propose a revised mechanism by which I-FABP may acquire and release fatty acid. We refer to this mechanism as the "dynamic portal hypothesis" and describe it according to its four key features:

(1) Fatty acid enters I-FABP through a locally disordered region of the protein backbone involving the C-terminal portion of helix II, the preceding α-II/$\beta$-B linker, and the C−D and E−F turns. Our current view of the "portal" is that of a flexible region of the protein backbone capable of undergoing large amplitude fluctuations, rather than a narrow channel modulated primarily by the rotations of a few side chains such as Phe-55. Although the X-ray crystal structures of I-FABP provided little direct evidence for the portal, the likely location was originally deduced by considering the region that would require the least conformational adjustment to admit a fatty acid into the internal cavity (Sacchettini *et al*., 1989a). The NMR results reinforce this proposed location for the portal and provide direct evidence that this region of I-FABP is disordered and flexible in solution. The localized backbone disorder observed in the NMR structure of apo-I-FABP may also help to explain the results of limited proteolysis experiments performed with proteins related to I-FABP (Jamison *et al.*, 1994). These experiments demonstrated that the apoproteins were more susceptible to proteolysis than their holoprotein counterparts, particularly in helix II. The proteolysis results were interpreted as a ligand-induced conformational change, envisioned as a rigid-body rotation of the intact helix−turn−helix domain relative to the $\beta$-barrel. Our current view of the conformational change is that of an order−disorder transition with a decoupling of the interactions between helix II and the C−D turn and an unraveling of helix II at the C-terminal end.

(2) The binding of fatty acid shifts the order−disorder equilibrium toward the ordered or closed state by stabilizing a series of cooperative interactions resembling a C-terminal helix capping box. Capping boxes are specific structural motifs found at helix termini (Baker & Hubbard, 1984; Richardson & Richardson, 1988; Presta & Rose, 1988; Dasgupta & Bell, 1993; Harper & Rose, 1993; Aurora *et al.*, 1994; Seale *et al.*, 1994). The middle of an α-helix is characterized by a pattern of successive hydrogen bonds between the backbone amide hydrogen of residue *i* and the carbonyl oxygen of residue $i - 4$. However, the first four amide hydrogens and the last four carbonyl oxygens of an α-helix are left without intrahelical backbone hydrogen-bonding partners. These positions are often satisfied by additional "capping" hydrogen bonds, sometimes contributed by protein side chains located in the turn segments bracketing the helix termini. Additionally, a hydrophobic interaction between residues immediately adjacent to the box on either side represents an integral component of the capping motif (Seale *et al.*, 1994). Experimental studies have revealed that the presence of a capping box sequence in peptides prevents fraying or unraveling of helices from their ends (Lyu *et al.*, 1993) and controls the point of helix initiation (Zhou *et al.*, 1994).

The sequence determinants and precise structures of various capping boxes have been described for both the N- and C-termini of α-helices (Harper & Rose, 1994; Aurora *et al.*, 1994; Seale *et al.*, 1994). One such capping box is known as the Schellman motif and is exemplified in I-FABP by the interactions stabilizing the C-terminus of α-helix I. The capping box includes backbone−backbone hydrogen bonds between M18 and I23 (defined as the C3 and C″ residues, respectively) and between E19 and G22 (C2 and C′). It also includes a hydrophobic interaction involving the side chains of M18 and I23 and the necessary left-handed conformation for the C′ residue, G22. According to the consensus CSI in Figure 1, helix I extends from residues 15 to 22 in both apo- and holo-I-FABP. Since these Schellman-type helix capping interactions are short-range and encoded in the protein sequence, it is not suprising that they are largely unaffected by the binding of fatty acid. Hence, the C-terminus of helix I is stable in both apo- and holo-I-FABP.

We propose that a somewhat analogous series of capping interactions stabilize the C-terminus of helix II, as schematized in Figure 7. However, these interactions are unlike the typical C-capping motifs described to date in that they involve residues far apart in the protein sequence and appear to be stabilized by the bound fatty acid. In holo-I-FABP, helix II extends from residues V25 to A32, and N24 represents a boundary residue. An analysis of hydrogen-bonding patterns in both the X-ray and NMR structures of I-FABP complexed with palmitate revealed the expected pattern of *i* to $i + 4$ hydrogen bonds for the carbonyl oxygens of residues N24−R28. The last turn of the helix contains K29−A32; H33 represents a boundary residue between the helix proper and the following turn generally referred to as the $C_{cap}$ residue. The conformation of these last four helical residues and the $C_{cap}$ residue are stabilized by capping interactions. The carbonyl oxygen of K29 is hydrogen-bonded to the side-chain imino proton of H33. An *i* to $i + 3$ backbone hydrogen bond occurs between the carbonyl oxygen of L30 and the backbone amide hydrogen of H33. There is no apparent hydrogen bond observed for the carbonyl oxygen of G31. Finally, the carbonyl oxygen of A32 hydrogen-bonds with the side-chain amide from N11.

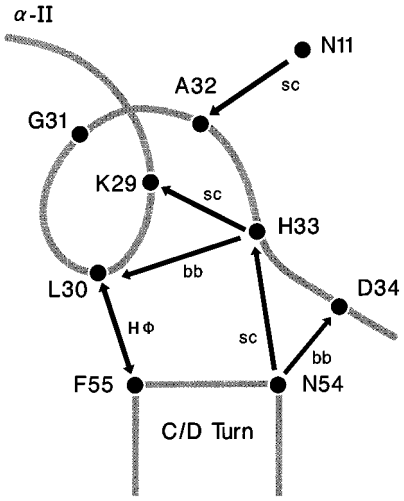


FIGURE 7: Proposed local and long-range capping interactions that stabilize the C-terminus of helix II in the tertiary structure of holo-I-FABP. Unidirectional arrows specify hydrogen bonds originating from either side-chain (sc) or backbone (bb) amide hydrogens and involving the backbone carbonyl oxygens of the residues directed by the arrows. A single bidirectional arrow illustrates the hydrophobic interaction between the side chains of residues F55 and L30. We propose that the bound fatty acid stabilizes these interactions via the side chain of F55.

Although the backbone dihedral angles of $C_{cap}$ residues typically deviate from helical averages, helical hydrogen-bonding patterns often extend to these residues (Aurora *et al.*, 1994; Seale *et al.*, 1994). In I-FABP, a long-range hydrogen bond from the turn between β-strands C and D appears to stabilize the $C_{cap}$ residue, H33. As shown in Figure 7, the side-chain amide hydrogen of N54 bonds with the backbone carbonyl oxygen of H33. As well, the backbone amide hydrogen of N54 participates in a bond to the backbone carbonyl oxygen of D34. To complete the motif, a hydrophobic interaction between residues bracketing the capping box is required. The aromatic ring of F55, also from the C−D turn, forms van der Waals contacts with the length of the hydrophobic side chain of L30. Together, residues N54 and F55 participate in long-range or tertiary "capping interactions" with the C-terminus of helix II and may be necessary for its stabilization.

The location of discrete disorder in the NMR results precisely mirrors the sequence requirements for helix capping interactions. The disorder in apo-I-FABP was most pronounced in residues 29−36, which includes the last four residues of helix II in the holoprotein. In addition, backbone disorder was observed in the turn between β-strands C and D, comprising residues 54−57. The capping interactions which apparently stabilize the C-terminus of helix II of the holo structure (Figure 7) are weakened in the apo structure. Positions 14−16 at the methyl end of the bound palmitate are involved in hydrophobic interactions with F55 as well as two other residues in the helical domain, I23 and K27. The side chain of Phe-55 has been proposed to serve as a lid that covers the entrance to the fatty acid portal (Sacchettini et al., 1989a, 1992; Banaszak *et al.*, 1994). The capping model in Figure 7 implies that F55 is not simply a lid but plays a central role in the order−disorder equilibrium by coupling fatty acid binding with helix stabilization. In this manner, fatty acid binding induces a series of cooperative

interactions that cap the C-terminus of helix II, shift the equilibrium toward the ordered state, and close the dynamic portal.

(3) Residue 54, which exhibits polymorphism in human I-FABP, participates in the proposed C-terminal capping interactions for α-helix II. As implied by the model in Figure 7, the order−disorder transition in the structure of I-FABP in solution may also be influenced by residue 54. In the rat protein, residue 54 is Asn, whereas in human I-FABP it is either Thr or Ala. An examination of aligned iLBP sequences (Banaszak *et al.*, 1994; Veerkamp & Maatman, 1995) reveals that residue 54 nearly always contains a side chain that can serve as a hydrogen-bond donor, typically Thr or Asn. One of the few exceptions is the A54 variant of human I-FABP, which might be expected to have a somewhat destabilized helix II compared with the Thr variant. The resulting shift in the order−disorder equilibrium for apo-I-FABP in solution might affect the rate and affinity of fatty acid binding. Oleate appears to bind to the Ala variant with a 2-fold higher $K_d$ compared with the Thr variant (Baier *et al.*, 1995). The weaker binding for the A54 variant of human I-FABP may result from an increased ligand dissociation rate because of increased disorder in the dynamic portal.

The polymorphism in human I-FABP was unexpectedly discovered in a search for genetic markers of insulin resistance and Type II diabetes in the Pima Indian population of the southwestern U.S. (Prochazka *et al*., 1993). Individuals hetero- or homozygous for the Thr allele were found to have higher rates of insulin resistance and fat oxidation (Baier *et al*., 1995). It is not known whether a causal relationship exists between the polymorphism at position 54 of I-FABP and insulin resistance, and it is not immediately obvious how this single amino acid variability in I-FABP might lead to a phenotypic tendency toward insulin resistance. However, it is well-established that high-fat diets induce insulin resistance in rats (Storlien *et al*., 1986, 1987, Grundleger & Thenen, 1982; Kim *et al*., 1996a), and I-FABP is likely to be involved in the absorption and/or transport of dietary fats (Sweetser *et al*., 1987; Kaikaus *et al*., 1990). The current observation that residue 54 may help regulate the order−disorder transition, and possibly the entry and exit of fatty acid, provides support for the concept that the polymorphism in human I-FABP could have significant metabolic consequences (Baier et al., 1995). Further studies are required to clarify the influence of this residue on the cooperative interactions described above and on ligand binding and transfer rates.

(4) The release of fatty acid from holo-I-FABP may be catalzyed by any process that destablizes the C-terminal capping interactions for helix II and shifts the order−disorder equilibrium toward the disordered state. One such process might be a collision between the holo-I-FABP complex and target sites on intracellular organelles such as smooth endoplasmic reticulum. A collision-mediated mechanism for the transfer of fatty acids from lipid-binding proteins to acceptor membranes has been proposed by Storch and colleagues (Herr *et al.*, 1995, 1996). A discussion of the possible role of the dynamic portal in the collision-mediated transfer of fatty acids is presented elsewhere (Hodsdon & Cistola, 1997).

In summary, we hypothesize that the destabilization of long-range interactions between the C-terminal half of helix II and the C−D turn in apo-I-FABP create a flexible backbone and a dynamic portal that permit the entry of fatty acid. Once bound, the fatty acid induces a series of cooperative interactions that stabilize this region, cap the helix, and close the ligand entry portal. In this manner, fatty acid-induced ordering of the backbone may effectively lower the dissociation rate and raise the binding affinity. Any subsequent process that destabilizes this region of the fatty acid−protein complex, such as a collision with target sites on organelles, may lead to an increased dissociation rate, decreased affinity, and a facilitated release of the ligand to the target organelle. Thus, I-FABP may possess a mechanism for adjusting its fatty acid binding affinity and dissociation rate based upon its interactions with specific cellular sites and for preferentially targeting fatty acids to those sites.

It is important to emphasize that the NMR and X-ray crystal structures of apo- and holo-I-FABP describe various end states of the binding process but not the binding reaction itself. Delineation of the residues that participate in the ligand entry mechanism will ultimately require measurements that directly monitor the binding reaction. Site-specific mutations of residues thought to participate in the dynamic portal and capping box interactions have been generated, and structural, kinetic, and thermodynamic analyses of ligand binding are underway.

## ACKNOWLEDGMENT

We are indebted to Drs. Jay Ponder for valuble advice and software for the structure calculations, Changguo Tang for NMR assistance, and James Toner for the biosynthesis and purification of the protein samples. Software for the analysis of chemical shift indices was generously provided by Drs. David Wishart and Brian Sykes, and for the analysis of protein structure quality, by Drs. Roman Laskowski, Janet Thornton, and Ton Rullman.

## SUPPORTING INFORMATION AVAILABLE

Five tables containing current $^{1}H$, $^{13}C$, and $^{15}N$ resonance assignments for apo- and holo-I-FABP (11 pages). Ordering information is given on any current masthead page.

## REFERENCES

Aurora, R., Srinivasan, R., & Rose, G. D. (1994) *Science 264*, 1126−1130.

Baier, L. J., Sacchettini, J. C., Knowler, W. C., Eads, J., Paolisso, G., Tataranni, P. A., Mochizuki, H., Bennett, P., Bogardus, C., & Prochazka, M. (1995) *J. Clin. Invest. 95*, 1281−1287.

Baker, E. N., & Hubbard, R. E. (1984) *Prog. Biophys. Mol. Biol. 44*, 97−179.

Banaszak, L. J., Winter, N., Xu, Z., Bernlohr, D. A., Cowan, S., & Jones, T. A. (1994) *Adv. Protein Chem.* 45, 89−151.

Cistola, D. P., Kim, K., Rogl, H., & Frieden, C. (1996) *Biochemistry 35*, 7559−7565.

Cowan, S. W., Newcomer, M. E., & Jones, T. A. (1993) *J. Mol. Biol. 230*, 1225−1246.

Dasgupta, S., & Bell, J. A. (1993) *Int. J. Pept. Protein Res. 41*, 499−511.

Fujiwara, T., Anai, T., Kurihara, N., & Nagayama, K. (1993) *J. Magn. Reson. A104*, 103−105.

Grundleger, M. L., & Thenen, S. W. (1982) *Diabetes 31*, 232−237.

Harper, E. T., & Rose, G. D. (1993) *Biochemistry 32*, 7605−7609.

Havel, T. F. (1991) *Prog. Biophys. Mol. Biol. 56*, 43−78.

Herr, F., Matarese, V., Bernlohr, D. A., & Storch, J. (1995) *Biochemistry 34*, 11840−11845.

Herr, F., Aronson, J., & Storch, J. (1996) *Biochemistry 35*, 1296−1303.

Hodsdon, M. E., & Cistola, D. P. (1997) *Biochemistry* (in press).

Hodsdon, M. E., Toner, J. J., & Cistola, D. P. (1995) *J. Biomol. NMR 6*, 198−210.
Hodsdon, M. E., Ponder, J. W., & Cistola, D. P. (1996) *J. Mol. Biol. 264*, 585−602.
Jamison, R. S., Newcomer, M. E., & Ong, D. E. (1994) *Biochemistry 33*, 2873−2879.
Kaikaus, R. M., Bass, N. M., & Ockner, R. K. (1990) *Experientia 46*, 617−630.
Kim, J. K., Wi, J. K., & Youn, J. H. (1996a) *Diabetes 45*, 651−658.
Kim, K., Cistola, D. P., & Frieden, C. (1996b) *Biochemistry 35*, 7553−7558.
Kraulis, P. (1991) *J. Appl. Crystallogr. 24*, 946−950.
LaLonde, J. M., Bernlohr, D. A., & Banaszak, L. J. (1994) *Biochemistry 33*, 4885−4895.
Laskowski, R., MacArthur, M. W., Moss, D. S., & Thornton, J. M. (1993) *J. Appl. Crystallogr. 26*, 283−291.
Lassen, D., Lücke, C., Kveder, M., Mesgarzadeh, A., Schmidt, J. M., Specht, B., Lezius, A., Spener, F., & Rüterjans, H. (1995) *Eur. J. Biochem. 230*, 266−280.
Lücke, C., Zhang, F., Rüterjans, H., Hamilton, J. A., & Sacchettini, J. C. (1966) *Structure 4*, 785−800.
Lyu, P. C., Liff, M. I., Marky, L. A., & Kallenbach, N. R. (1993) *Biochemistry 32*, 669−673.
Matarese, V., Stone, R. L., Waggoner, D. W., & Bernlohr, D. A. (1989) *Prog. Lipid Res. 28*, 245−272.
Morris, A. L., MacArthur, M. W., Hutchinson, E. G., & Thornton, J. M. (1993) *J. Appl. Crystallogr. 26*, 283−291.
Ockner, R. A., Manning, J. A., Poppenhausen, R. B., & Ho, W. K. L. (1972) *Science 177*, 56−58.
Presta, L. G., & Rose, G. D. (1988) *Science 240*, 1632−1641.
Prochazka, M., Lillioja, S., Tait, J. F., Knowler, W. C., Mott, D. M., Spraul, M., Bennett, P. H., & Bogardus, C. (1993) *Diabetes 42*, 514−519.
Richardson, J. S., & Richardson, D. C. (1988) *Science 240*, 1648−1652.
Rizo, J., Liu, Z.-P., & Gierasch, L. M. (1994) *J. Biomol. NMR 4*, 741−760.
Ropson, I. J., & Frieden, C. (1992) *Proc. Natl. Acad. Sci. U.S.A. 89*, 7222−7226.
Rullmann, J. A. C. (1996) AQUA, Computer Program, Department of NMR Spectroscopy, Bijvoet Center for Biomolecular Research, Utrecht University, Utrecht, The Netherlands.
Sacchettini, J. C., & Gordon, J. I. (1993) *J. Biol. Chem. 268*, 18399−18402.
Sacchettini, J. C., Gordon, J. I., & Banaszak, L. J. (1989a) *J. Mol. Biol. 208*, 327−339.
Sacchettini, J. C., Gordon, J. I., & Banaszak, L. J. (1989b) *Proc. Natl. Acad. Sci. U.S.A. 86*, 7736−7740.
Sacchettini, J. C., Scapin, G., Gopaul, D., & Gordon, J. I. (1992) *J. Biol. Chem. 267*, 23534−23545.
Scapin, G., Gordon, J. I., & Sacchettini, J. C. (1992) *J. Biol. Chem. 267*, 4253−4269.
Seale, J. W., Srinivasan, R., & Rose, G. D. (1994) *Protein Sci. 3*, 1741−1745.
Shaka, A. J., Keeler, J., Frenkiel, T., & Freeman, R. (1983) *J. Magn. Reson. 52*, 335−338.
Shaka, A. J., Barker, P. B., & Freeman, R. (1985) *J. Magn. Reson. 64*, 547−552.
Storlien, L. H., James, D. E., Burleigh, K. M., Chisholm, D. J., & Kraegen, E. W. (1986) *Am. J. Physiol. 251*, E576−E583.
Storlien, L. H., Kraegen, E. W., Chisholm, D. J., Ford, G. L., Bruce, D. G., & Pascoe, W. S. (1987) *Science 237*, 885−888.
Sweetser, D. A., Heuckeroth, R. O., & Gordon, J. I. (1987) *Annu. Rev. Nutr. 7*, 337−359.
Thompson, J. R., Bratt, J. M., & Banaszak, L. J. (1995) *J. Mol. Biol. 252*, 433−446.
Veerkamp, J. H., & Maatman, R. G. H. J. (1995) *Prog. Lipid Res. 34*, 17−52.
Winter, N. S., Gordon, J. I., & Banaszak, L. J. (1990) *J. Biol. Chem. 19*, 10955−10958.
Wishart, D. S., & Sykes, B. D. (1994) *J. Biomol. NMR 4*, 171−180.
Xu, Z., Bernlohr, D. A., & Banaszak, L. J. (1993) *J. Biol. Chem. 268*, 7874−7884.
Young, A. C. M., Scapin, G., Kromminga, A., Patel, S. B., Veerkamp, J. H., & Sacchettini, J. C. (1994) *Structure 2*, 523−534.
Zhou, H. X., Lyu, P., Wemmer, D. E., & Kallenbach, N. R. (1994) *Proteins: Struct., Funct., Genet. 18*, 1−7.

BI961890R